Supplementary Information: Mechanistic Insights into Photoinduced Energy and Charge Transfer Dynamics between Magnesium-Centered Tetrapyrroles and Carbon Nanotubes

Jia-Ning Zhou,[a,†] Ke-Qin Cheng,[a,†] Xiaolong Zhang,[a] Shubin Yang,[a] Jie Liu,[a] Wenzuo Li,[a] Qingzhong Li,[a] Juan Han,[b,*] Xiao-Ying Xie,[a,*] and Ganglong Cui[b,c]

[a]*The Laboratory of Theoretical and Computational Chemistry, School of Chemistry and Chemical Engineering, Yantai University, Yantai, 264005, China.*
[b]*Key Laboratory of Theoretical and Computational Photochemistry, Ministry of Education, College of Chemistry, Beijing Normal University, Beijing, 100875, China.*
[c]*Hefei National Laboratory, Hefei, 230088, China.*
[†]*The authors contribute equally.*

E-mail: hanjuan@bnu.edu.cn; xiaoying.xie@mail.bnu.edu.cn

Table of Contents

Simulation Methods

Nonadiabatic Dynamics Methods

Nonadiabatic carrier transfer dynamics simulations are carried out using Tully's fewest-switches surface-hopping methods based on density functional theory. [1-4] Time-dependent density functional theory in Kohn-Sham framework maps an interacting many-body system onto a system of noninteracting particles in which their electron densities equals to each other. As a result, time-dependent charge density $\rho(r,t)$ of an interacting system is obtained from a set of time-dependent Kohn–Sham orbitals $\psi_p(r,t)$ [5-9]

$$\rho(r,t) = \sum_{p=1}^{N_e} \left|\psi_p(r,t)\right|^2$$

Electron density evolution finally leads to a set of single-electron equations for evolution of Kohn–Sham orbitals $\psi_p(r,t)$ [10-14]

$$i\hbar \frac{\partial \psi_p(r,t)}{\partial t} = \hat{H}(r;R)\psi_p(r,t) \quad p = 1,2,\dots,N_e$$

If expanding time-dependent electron or hole wavefunction $\psi_p(r,t)$ in terms of interested unoccupied or occupied adiabatic Kohn–Sham orbitals $\phi_k(r,t)$ calculated from density functional theory calculations along adiabatic molecular dynamics trajectories

$$\psi_p(r,t) = \sum_k c_k(t)\phi_k(r;R)$$

one can obtain a set of equations of motion for expanding coefficients $c_j(t)$

$$i\hbar \frac{\partial c_j(t)}{\partial t} = \sum_k c_k(t)\left(\varepsilon_k \delta_{jk} - i\hbar d_{jk}\right)$$

where ε_k is energy of kth adiabatic state and d_{jk} is nonadiabatic coupling between adiabatic states j and k. The former is directly obtained from density functional theory calculations and the latter is calculated numerically through finite difference methods as overlaps of adiabatic states at times t and $t + \Delta t$:

$$d_{jk} = \left\langle \phi_j(r;R) \middle| \frac{\partial \phi_k(r;R)}{\partial t} \right\rangle \approx \frac{\langle \phi_j(t) | \phi_k(t+\Delta t) \rangle - \langle \phi_j(t+\Delta t) | \phi_k(t) \rangle}{2\Delta t}$$

in which $\phi_j(t)$ and $\phi_k(t+\Delta t)$ are wave functions of adiabatic states j and k at times t and $t+\Delta t$, respectively. Previous algorithms are primarily implemented with plane wave basis sets; [15-16] instead, we have recently implemented this nonadiabatic electron or hole dynamics method with Gaussian basis sets with CP2K [17-18] and have successfully applied to studying many materials. [19-22]

Carrier Transfer Analysis

To estimate electron or hole transfer from one to another fragment in nonadiabatic dynamics simulations, we have developed an efficient density-matrix based method. First, we can define a density matrix D in terms of atomic orbitals χ_μ

$$D_{\mu\nu i}(t) = p_i(t)\chi_{\mu i}\chi_{\nu i}^*$$

in which $p_i(t)$ is time-dependent occupation number of the ith adiabatic state calculated on the basis of above expanding coefficients $c_i(t)$; $\chi_{\mu i}$ is the μth atomic orbital coefficient of the ith adiabatic state. Similar to Mulliken charge analysis, [23] we have then defined a population matrix P using density matrix D and atomic overlap matrix S

$$P_{\mu\nu i} = D_{\mu\nu i}S_{\mu\nu}$$

Finally, we can obtain the ath atomic charge through summing all basis functions μ belonging to that atom and all involved adiabatic states i

$$P_a = \sum_i \left(\sum_{\mu\in a,\nu\in a} P_{\mu\nu i} + \frac{1}{2}\left(\sum_{\mu\in a,\nu\notin a} P_{\mu\nu i} + \sum_{\mu\notin a,\nu\in a} P_{\mu\nu i} \right) \right)$$

It should be noted that if only an atomic orbital belongs to the ath atom, just half of $P_{\mu\nu i}$ is used, as done by Mulliken charge analysis method. [21] Accordingly, total electron on a fragment A is done by summing all atomic charges belonging to that fragment

$$P_A = \sum_i p_i(t) P_{Ai}$$

in which

$$P_{Ai} = \sum_{a \in A} \left(\sum_{\mu \in a, \nu \in a} \chi_{\mu i} \chi_{\nu i}^* S_{\mu\nu} + \frac{1}{2} \left(\sum_{\mu \in a, \nu \notin a} \chi_{\mu i} \chi_{\nu i}^* S_{\mu\nu} + \sum_{\mu \notin a, \nu \in a} \chi_{\mu i} \chi_{\nu i}^* S_{\mu\nu} \right) \right)$$

In such a case, the differentiation of P_A is then derived as

$$\mathrm{d}P_A = d\left(\sum_i c_i^* c_i P_{Ai} \right) = \sum_i (d(c_i^* c_i) P_A + c_i^* c_i dP_{Ai})$$

in which the first term has variational occupations for adiabatic states i and the second term has constant adiabatic state occupations but changeable electron population. These two terms correspond to nonadiabatic and adiabatic electron transfer contributions. The former is mainly caused by state hoppings between different adiabatic states and the latter is primarily originated from changes of adiabatic states induced by atomic motions. Finally, it should be noted that Gaussian basis sets are used in our simulations, so molecular coefficients $\chi_{\mu i}$ are real numbers. Adiabatic states' expanding coefficients $c_i(t)$ are complex numbers, but they are not directly used; instead, their $c_i(t)c_i^*(t)$ products are used for calculating time-dependent occupation number $p_i(t)$ of the ith adiabatic state, which is a real number.

Excitonic Effects in the MgP@SWNT Heterojunction

Excitonic effects are important; however, LR-TDDFT and GW/BSE that take excitonic effects into consideration are very expensive for nonadiabatic simulations. [24-26] Instead, we have compared the excitation energies by LR-TDDFT and the energy differences by DFT from 11 pairs of random structures from the NVE trajectory. As shown in Fig. S7, a very good linear relationship is obtained, which proves that DFT-based NAMD simulations can provide accurate results for our studied systems. In fact, many previous works have demonstrated that some dynamical processes are less influenced by excitonic effects. [27-31]

Additional Figures

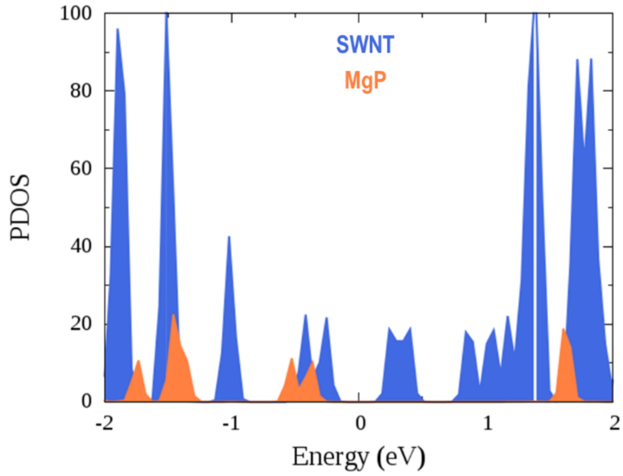

Fig. S1 The PDOS of MgP@SWNT with a supercell (1×1×5) containing a total of 437 atoms.

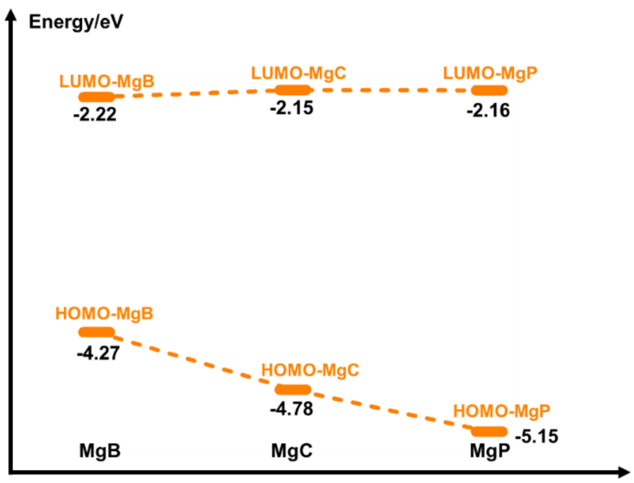

Fig. S2 The energy levels of HOMO and LUMO within MgBC, MgC, and MgP.

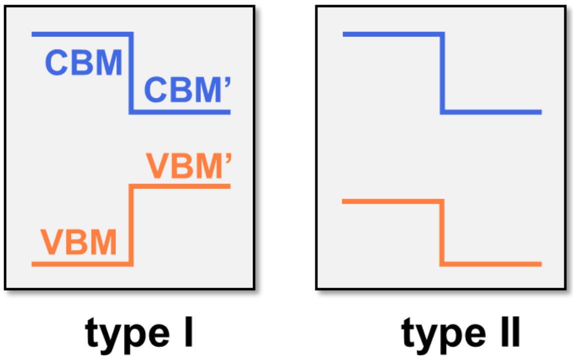

Fig. S3 Schematic definition of the type-I and type-II heterojunctions widely used in the discipline of condensed matter.

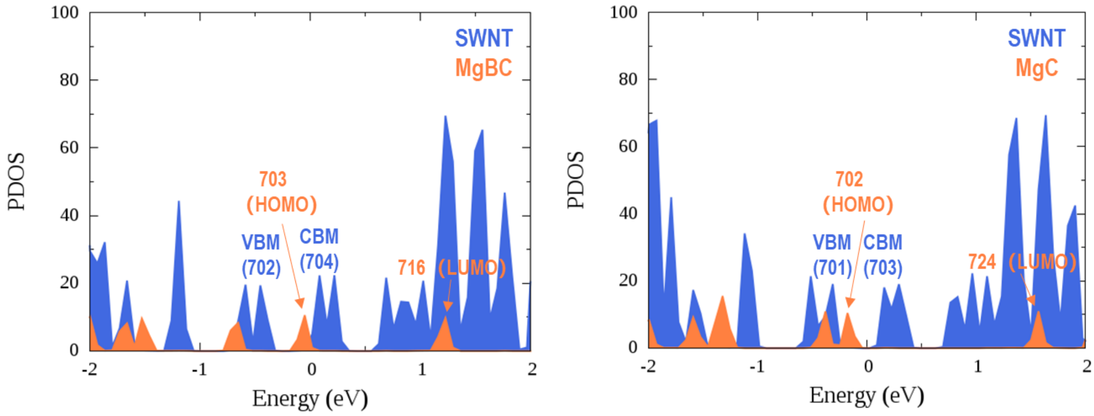

Fig. S4 The PDOS of MgBC@SWNT (left) and MgC@SWNT (right) calculated at PBE+D3 level.

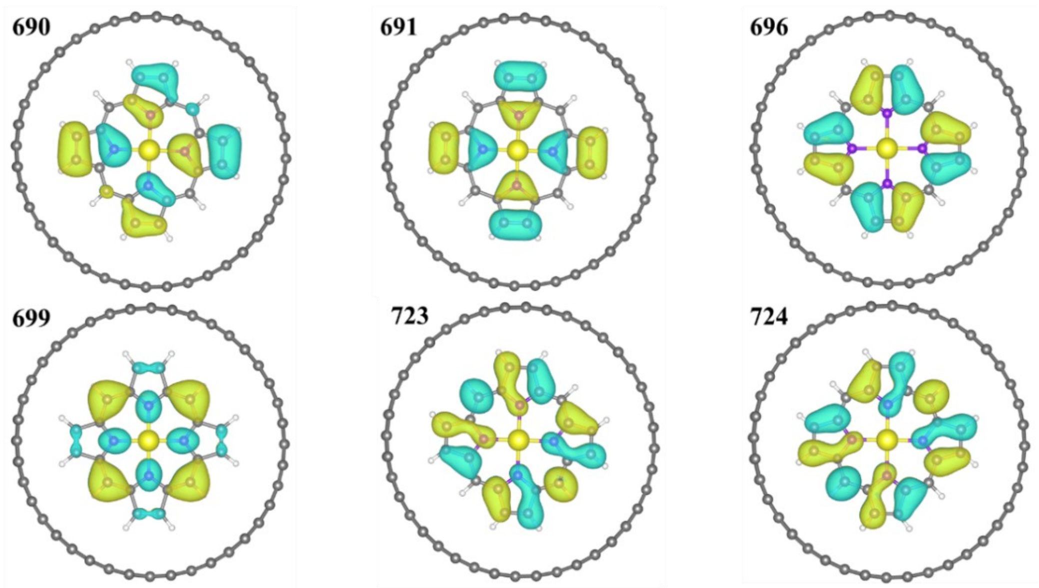

Fig. S5 Spatial distributions of photogenerated electron and hole initially populated states upon excitation of MgP@SWNT heterojunction.

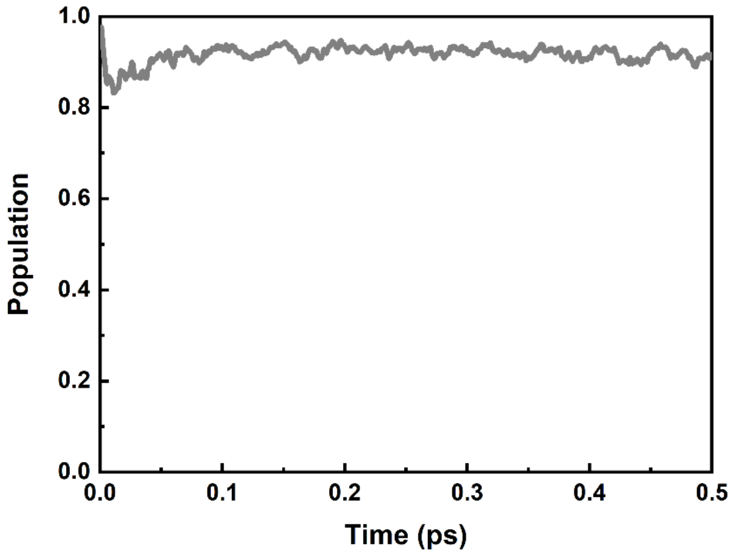

Fig. S6 The first 0.5 ps of time-dependent hole population on MgP in nonadiabatic dynamics simulations from the HE excitation.

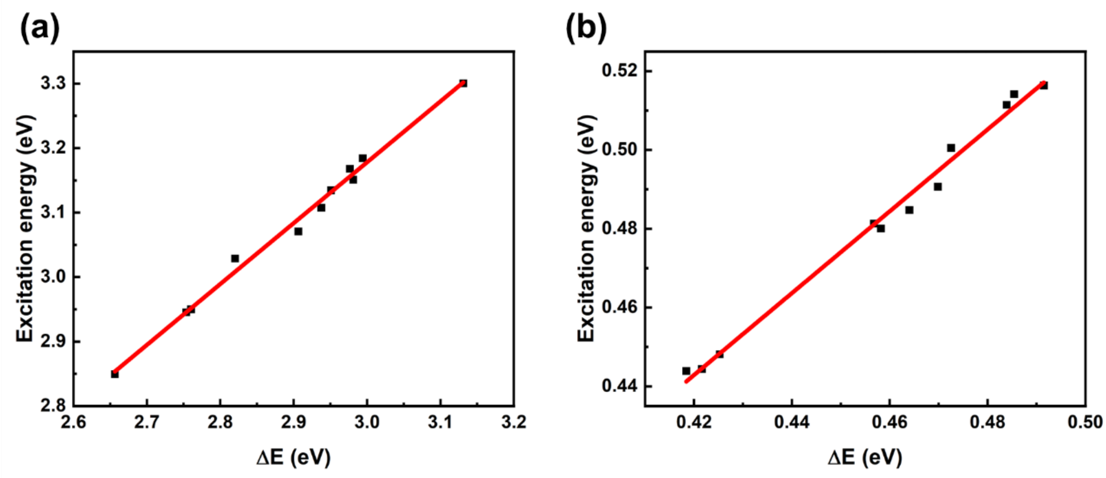

Fig. S7 The linear relationship between excitation energies by LR-TDDFT and energy differences between two involved states by DFT calculations in MgP (a) and SWNT (b).

Additional Tables

Table S1. Calculated Interfragment Interaction Function (δg^{inter}) and Binding Energy ($E_{binding}$, eV) of Functionalized SWNT with MgBC, MgC, and MgP Implant Perpendicular or Parallel to the Axis of the Nanotube.

	MgBC@SWNT		MgC@SWNT		MgP@SWNT	
	perpendicular	parallel	perpendicular	parallel	perpendicular	parallel
δ_g^{inter}	0.78	0.29	0.77	0.28	0.75	0.20
$E_{binding}$	1.83	1.05	1.65	0.98	1.37	0.56

Table S2. Vertical Excitation Energies (E, in eV), Oscillator Strengths (Osc.) and Main Electronic Configuration of the Lowest Four Singlet States of MgP Calculated with LR-TDDFT.

State	E	Osc.	Electronic Configuration
1	2.314	1.55566E-04	HOMO→LUMO+1 39.7% HOMO-1→LUMO 35.3% HOMO→LUMO 11.7% HOMO-1→LUMO+1 10.3%
2	2.315	1.53514E-04	HOMO→LUMO 39.7% HOMO-1→LUMO+1 35.3% HOMO→LUMO+1 11.6% HOMO-1→LUMO 10.4%
3	3.206	1.01290E-02	HOMO-2→LUMO 94.5%
4	3.207	1.03056E-02	HOMO-2→LUMO+1 95.2%

References

1. C. F. Craig, W. R. Duncan, O. V. Prezhdo, Trajectory Surface Hopping in the Time-Dependent Kohn-Sham Approach for Electron-Nuclear Dynamics. *Phys. Rev. Lett.*, 2005, **95**, 163001.
2. J. C. Tully, R. K. Preston, Trajectory Surface Hopping Approach to Nonadiabatic Molecular Collisions: The Reaction of H^+ with D_2. *J. Chem. Phys.*, 1971, **55**, 562-572.

3. S. Hammes-Schiffer, J. C. Tully, Proton Transfer in Solution: Molecular Dynamics with Quantum Transitions. *J. Chem. Phys.*, 1994, **101**, 4657–4667.
4. A. V. Akimov, A. J. Neukirch, O. V. Prezhdo, Theoretical Insights into Photoinduced Charge Transfer and Catalysis at Oxide Interfaces. *Chem. Rev.*, 2013, **113**, 4496–4565.
5. P. Hohenberg, W. Kohn, Inhomogeneous Electron Gas. *Phys. Rev.*, 1964, **136**, B864–B871.
6. W. Kohn, L. J. Sham, Self-Consistent Equations Including Exchange and Correlation Effects. *Phys. Rev.*, 1965, **140**, A1133-A1138.
7. R. G. Parr, W. T. Yang, Density-Functional Theory of Atoms and Molecules; *Oxford University Press,* 1994.
8. K. Fiolhais, F. Nogueira, M. Marques, A Primer in Density Functional Theory; *Springer: Berlin,* 2003.
9. M. A. L. Marques, C. A. Ullrich, F. Nogueira, A. Rubio, K. Burke, E. K. U. Gross, Time-dependent Density Functional Theory; *Springer: Berlin,* 2006.
10. I. Franco, S. Tretiak, Electron-Vibrational Dynamics of Photoexcited Polyfluorenes. *J. Am. Chem. Soc.*, 2004, **126**, 12130-12140.
11. M. A. L. Marques, E. K. U. Gross, Time-Dependent Density Functional Theory. *Annu. Rev. Phys. Chem.*, 2004, **55**, 427-455.
12. M. A. L. Marques, X. López, D. Varsano, A. Castro, A. Rubio, Time-Dependent Density-Functional Approach for Biological Chromophores: The Case of the Green Fluorescent Protein. *Phys. Rev. Lett.*, 2003, **90**, 258101.
13. S. Tretiak, K. Igumenshchev, V. Chernyak, Exciton Sizes of Conducting Polymers Predicted by Time-Dependent Density Functional Theory. *Phys. Rev. B: Condens. Matter Mater. Phys.*, 2005, **71**, 033201.
14. R. Baer, T. Seideman, S. Ilani, D. Neuhauser, Ab Initio Study of the Alternating Current Impedance of a Molecular Junction. *J. Chem. Phys.*, 2004, **120**, 3387-3396.
15. A. V. Akimov, O. V. Prezhdo, Nonadiabatic Dynamics of Charge Transfer and Singlet Fission at the Pentacene/C_{60} Interface. *J. Am. Chem. Soc.*, 2014, **136**,

1599-1608.

16. A. V. Akimov, O. V. Prezhdo, The PYXAID Program for Non-Adiabatic Molecular Dynamics in Condensed Matter Systems. *J. Chem. Theory Comput.*, 2013, **9**, 4959-4972.

17. J. Hutter, M. Iannuzzi, F. Schiffmann, J. VandeVondele, CP2K: Atomistic Simulations of Condensed Matter Systems. *WIREs Comput. Mol. Sci.*, 2014, **4**, 15-25.

18. J. VandeVondele, M. Krack, F. Mohamed, M. Parrinello, T. Chassaing, J. Hutter, QUICKSTEP: Fast and Accurate Density Functional Calculations Using a Mixed Gaussian and Plane Waves Approach. *Comput. Phys. Commun.*, 2005, **167**, 103-128.

19. X.-Y. Liu, X.-Y. Xie, W.-H. Fang, G. Cui, Theoretical Insights into Interfacial Electron Transfer between Zinc Phthalocyanine and Molybdenum Disulfide. *J. Phys. Chem. A*, 2018, **122**, 9587-9596.

20. X.-Y. Liu, W.-K. Chen, W.-H. Fang, G. Cui, Nonadiabatic Dynamics Simulations Reveal Distinct Effects of the Thickness of PTB7 on Interfacial Electron and Hole Transfer Dynamics in PTB7@MoS_2 Heterostructures., *J. Phys. Chem. Lett.*, 2019, **10**, 2949-2956.

21. X.-Y. Xie, X.-Y. Liu, Q. Fang, W.-H. Fang, G. Cui, Photoinduced Carrier Dynamics at the Interface of Pentacene and Molybdenum Disulfide. *J. Phys. Chem. A*, 2019, **123**, 7693-7703.

22. J.-J. Yang, X.-Y. Liu, W.-H. Fang, D. Xiao, G. L. Cui, Photoinduced Carrier Dynamics at the Interface of Black Phosphorus and Bismuth Vanadate. *J. Phys. Chem. A*, 2019, **123**, 10019-10029.

23. R. S. Mulliken, Electronic Population Analysis on LCAO-MO Molecular Wave Functions. I. *J. Chem. Phys.*, 1955, **23**, 1833-1840.

24. X. Jiang, Q. Zheng, Z. Lan, W. A. Saidi, X. Ren, J. Zhao, Real-Time GW-BSE Investigations on Spin-Valley Exciton Dynamics in Monolayer Transition Metal Dichalcogenide. *Sci. Adv.*, 2021, **7**, eabf3759.

25. X. Zhang, G. Lu, R. Baer, E. Rabani, D. Neuhauser, Linear-Response Time-

Dependent Density Functional Theory with Stochastic Range-Separated Hybrids. *J. Chem. Theory Comput.*, 2020, **16**, 1064-1072.

26. J. Liu, Z. Li, X. Zhang, G. Lu, Unraveling Energy and Charge Transfer in Type-II van der Waals Heterostructures. *NPJ Comput. Mater.*, 2021, **7**. 191.
27. R. Long, O. V. Prezhdo, Asymmetry in the Electron and Hole Transfer at a Polymer-Carbon Nanotube Heterojunction. *Nano Lett.*, 2014, **14**, 3335-3341.
28. R. Sarkar, M. Habib, S. Pal, O. V. Prezhdo, Ultrafast, Asymmetric Charge Transfer and Slow Charge Recombination in Porphyrin/CNT Composites Demonstrated by Time-Domain Atomistic Simulation. *Nanoscale,* 2018, **10**, 12683-12694.
29. J.-J. Yang, Z.-W. Li, X.-Y. Liu, W.-H. Fang, G. Cui, Photoinduced Electron Transfer from Carbon Nanotubes to Fullerenes: C_{60}versus C_{70}. Phys. *Chem. Chem. Phys.*, 2020, **22**, 19542-19548.
30. X.-Y. Xie, J.-J. Yang, X.-Y. Liu, Q. Fang, W.-H. Fang, G. Cui, Interfacial Photoinduced Carrier Dynamics Tuned by Polymerization of Coronene Molecules Encapsulated in Carbon Nanotubes: Bridging Type-I and Type-II Heterojunctions. *Phys. Chem. Chem. Phys.*, 2021, **23**, 13503-13511.
31. Y. Lei, Z. Zheng, L. Vasquez, J. Zhao, J. Ma, H. Ma, Enhanced Electron Transfer and Spin Flip through Spin–Orbital Couplings in Organic/Inorganic Heterojunctions: A Nonadiabatic Surface Hopping Simulation. *J. Phys. Chem. Lett.,* 2022, **13**, 4840-4848.